Forecast Model Applications of Retrieved Three Dimensional Liquid Water Fields

By

William H. Raymond and William S. Olson

Cooperative Institute for Meteorological Satellite Studies

1225 West Dayton Street

University of Wisconsin

Madison, Wisconsin 53706

To be modified and submitted to *J. Appl. Meteor.*

Abstract

Retrieved three dimensional liquid water fields are used in a regional mesoscale forecast model to help induce storm development and enhance the early production of precipitation. Vertical layer-mean heating rates are regressed against slant path-integrated liquid and ice precipitating water contents, based upon a cloud ensemble model. This procedure yields a best fit two-parameter regression formula for each vertical layer. The regression formulae are used to estimate latent heating values from the slant-path integrated liquid and ice precipitation water contents from SSM/I retrievals. In the forecast model, diabatic temperature contributions are calculated and used in a diabatic forcing procedure with or without diabatic initialization. We find that the time needed to spin-up precipitation processes in tropical storm Emily is greatly accelerated, and the horizontal distribution of the forecast fields is improved through the application of the data.

1. Introduction

Mesoscale forecasts must go through a development stage when initial conditions do not adequately resolve mesoscale circulations. This spin-up is common in numerical weather prediction since much of the data is obtained from synoptic scale observations. Also, the failure to include cloud, rain and ice fields in the assimilation procedure means than this spin-up process is repeated with the next sequential forecast. This neglect is a natural consequence since cloud and rain water data have been unavailable. There has been some effort to circumvent this problem through the use of diabatic or cumulus initialization techniques (Errico and Rasch 1988; Donner 1988; Turpeinen et al. 1990; Tarbell et al 1981; Salmon and Warner 1986, etc.). These procedures have been somewhat successful, but the vertical distribution of the diabatic heating remains a major problem since raingauge reports give a measure of surface precipitation depth, and visible/infrared remote sensing methods typically yield estimates of surface rain rate.

Some success in assimilating explicit cloud and rain water information, and initializing diabatic processes was demonstrated in chapter one of this report. A continuation of these procedures is presented here, but using radiance data measured by the Special Sensor Microwave/Imager (SSM/I) to estimate the heating rates. SSM/I-derived estimates of integrated precipitating liquid and ice are optimized using physical information supplied by a cloud ensemble/radiative model of convective and stratiform clouds. Vertical layer-mean latent heating rates from the cloud ensemble model are regressed against the slant path-integrated liquid and ice precipitation water contents to determine the best fit two parameter regression coefficients for each vertical layer. Given SSM/I retrievals of path integrated liquid and ice precipitation amounts, the regression formulae yields a vertical distribution of heating rates for our forecast model applications.

In this final report only the data associated with tropical storm Emily is evaluated. This will be expanded in the near future for a proposed journal article. Forecasts are made using the National Meteorological Centre's (NMC) initialized global analyses. When only an adiabatic initialization is used, our forecasts produce no development in the vicinity of the Emily disturbance. This result

suggests that the initial data are missing most of the mesoscale information needed to begin the storm development. Forecasts are dramatically different when either diabatic forcing or diabatic forcing combined with diabatic initialization is used. These findings are presented and discussed in this portion of the final report, but first, additional details about the three dimensional diabatic heating rate data are presented.

2. Latent Heating Rates for Emily at 1004 UTC, September 21, 1987

Latent heating rates in Emily at 1004 UTC, September 21, 1987 are derived from the SSM/I retrieval of the slant path-integrated precipitation liquid and ice distributions discussed in chapter 3 of this report. The latent heating analysis is based upon regression formulae which are applied to the retrieved precipitation fields. The regression formulae are derived as follows.

Latent heating rates from the convective and stratiform cloud simulations in each of the cloud ensembles of chapter 2 are interpolated to grid points within the 25 km x 25 km x 20 km domain shown in Fig 3 of that section. The heating rates are then averaged in 1.1 km thick layers over the 25 km x 25 km domain to obtain layer-mean estimates at 17 levels for each cloud ensemble. The layer-mean latent heating rates are regressed against the slant path-integrated liquid and ice precipitation water contents in the same ensemble using the formula

$$H_{lat}=a_1*PLWP + a_2*PIWP , \qquad (1)$$

where H_{lat} is the latent heating rate in joules/m^3-s, PLWP is the slant path-integrated liquid precipitation averaged over the grid box, PIWP is the slant path-integrated ice precipitation averaged over the grid box, and a_1 and a_2 are the best-fit regression coefficients. Both the slant path-integrated liquid and ice amounts are assumed to have units of kgm^{-2} in (1). PLWP and PIWP are chosen as predictors of the latent heating rate, since these parameters are estimated in the SSM/I physical retrieval method (see chapter 3). Note that H_{lat} in the above formula equals zero if both

PLWP and PIWP are zero, which is a constraint on the regression formula since it is assumed that their is no latent heating if no cloud or precipitation exist.

A total of 213 convective cloud ensembles and 42 stratiform cloud ensembles based upon the GATE day 261 environment (1200 UTC sounding from Quadra research vessel) are utilized in the regression analysis. The regression coefficients and formula errors for each of the 17 standard levels are summarized in Table 1. Note that at levels below the freezing level (4km), latent heating rates increase with the path-integrated precipitation liquid amount and decrease with the path-integrated precipitating ice amount. The negative correlation between latent heating rates and ice amount (negative values of a_2) can be linked to the differences between the thermodynamics of convection and stratiform precipitation. Low level heating is normally associated with convective precipitation events (Tao et al. 1990). However, if precipitating ice concentrations are high relative to precipitating liquid amounts, then a stratiform precipitation event is indicated. Stratiform precipitation is usually associated with cooling at altitudes below the freezing level, due to melting of precipitating ice and evaporation of rain.

At levels between 5.70 km and 10.70 km, the latent heating rate is positively correlated with both the liquid and ice precipitation amounts. At higher altitudes the magnitude of the latent heating rate fall off substantially, and it is difficult to infer any systematic trends. Latent heating rates at 17.45 km and 18.58 km are so low that meaningful regressions are not possible. It may also be noted that correlations between latent heating rate regression estimates and the true heating rates are significant at and below 10.70 km, with the exception of the 2.82 km and 3.94 km levels.

The latent heating rates are inferred from the slant-path integrated precipitating liquid and ice estimates obtained from the SSM/I physical retrieval method, upon inserting these estimates into the regression formula (1) above. The latent heating rates at the standard levels (see Table 1) are then interpolated to levels at 50 mb increments between 1000 mb and 100 mb inclusive. These vertically-interpolated values are then interpolated in the horizontal from the 25 km resolution swath grid to the 40 km resolution forecast model grid. The contour plot in Fig 1, superimposed on the GOES IR image valid at 1001 UTC 21 September 1987, shows the distribution of temperature

increase associated with latent heating at sigma level 10, approximately the 700 mb level, inferred from the 1004 UTC Emily retrieval (also see Figs 5a and 5b of chapter 3). Here the maximum latent heating produces a temperature change of 0.07 C per 300 s^{-1}. The bi-modal vertical distribution of the latent heating is largest at sigma levels 12 and 6, approximately at the 850 and 500 mb levels, where the maximum diabatic activity is equivalent to 0.44 C and 0.37 C per 300 s^{-1}, respectivity.

3. The Diabatic Procedure

A diabatic initialization and/or diabatic forcing procedure is installed into the CIMSS forecast model to take full advantage of the semi-implicit method, as previously described in chapter 1. This is accomplished by modifying the semi-implicit average temperature $T^{2\tau}$, computed from the thermodynamic equation (McGregor et al 1978; Leslie et al 1985), by adding the externally determined temperature contribution T_{ex}. This redefines the average temperature at the appropriate grid points according to

$$T^{2\tau} \equiv T^{2\tau} + T_{ex} , \tag{2}$$

where

$$T_{ex} = (L\Delta t/\rho c_p)H_{lat} , \tag{3}$$

and

$$T^{2\tau} = [T^{\tau+1} + T^{\tau-1}]/2 . \tag{4}$$

Here c_p is the specific heat for constant pressure, H_{lat} the remotely sensed heating rate determined by (1), L is the latent heat of condensation or evaporation and the superscripts signify the time step.

During the diabatic forcing or diabatic initialization process, which is designed to initialize the mesoscale circulation, the mixing ratio can be altered as desired To avoid excessive evaporation, some upward adjustment of the mixing ratio may be required, namely

$$q_v = q_v + \Delta q_v \,. \tag{5}$$

In our calculations Δq_v is set to give the equivalent of the amount of moisture needed in the condensation process to achieve the observed heating rates.

During the vertical mode initialization procedure (Bourke and McGregor 1983) T_{ex} is held constant at the selected grid points. The application early in the forecast period of an external diabatic forcing represents a natural extension of the diabatic initialization. This procedure requires at each time step that the grid point average temperature is modified by the difference between the external contribution T_{ex} and the model produced diabatic temperature $T_{IN} = |\Delta t L Q/c_p|$, yielding

$$T^{2\tau} \equiv T^{2\tau} + (T_{ex} - T_{IN}) \,. \tag{6}$$

Here Q is the model produced liquid water condensation at each grid point over one time step. In our study the quantity in parenthesis in (6) is taken to be non-negative. Equation (6) can be interpreted as a blending over time, between the forcing and the model diabatic production. If all precipitating grid locations have sufficient condensation, then the external forcing is reduced to zero. Even though this is the desired result it is not explicitly required before the termination of the forcing at a preselected forecast time. This application of the external forcing is somewhat modified from the procedure used in Newtonian nudging (Hoke and Anthes 1976).

Note that (2) and (6) are similar, except model produced condensation reduces the external forcing in (6). This reduction removes the potential for over forcing. The external diabatic forcing is a natural continuation of diabatic contributions introduced in the initialization. The forcing is

applied starting with the first time step after the vertical mode initialization and continued until the model produces an equivalent temperature change or until a preselected termination time is exceeded. With each passing time step, T_{ex} is advected by the model horizontal winds according to

$$\partial(T_{ex})/\partial t + u\partial(T_{ex})/\partial x + v\partial(T_{ex})/\partial y = 0. \qquad (7)$$

In regions with strong vertical shear it may be advantageous to advect T_{ex} using a vertically averaged horizontal wind. The advection process will ultimately smooth and diffuse the heating if (7) is used over a sufficiently large time period. Normally the diabatic forcing lasts only a few hours. In any event, some tapering must be used to terminate the diabatic forcing, provided (6) is not reduced to zero by model generated condensation processes. Remotely sensed time variations in T_{ex} could also be allocated for if known. In our calculations, T_{ex} is assumed to remain unchanged except for horizontal advection.

An alternative approach is to apply the external diabatic forcing at the satellite observation time. Then, a gradual transition into and exit from the external diabatic forcing regime greatly avoids the production of noise and gravity waves during the forecast. The time span needed to produce gradual changes depends upon the magnitude of the external forcing. The length of time period used in the forcing can be varied to achieve the desired result. Excessively long periods of forcing should be avoided since they can can lead to some negative consequences. For example, too much diabatic forcing can cause a build up of excessive amounts of liquid water that can eventually lead to large amounts of precipitation drag which cause downbursts that choke off the convergence and the moisture supply. Events of this type can reduce the overall storm development because they may produce storm-wide low level divergence that chokes off the moisture supply.

4. Forecasting Emily

In Figs 2 and 3 are 700 mb geopotential heights and divergence fields from a twenty four hour forecast beginning at 0000 UTC 21 September 1987. These fields are super-imposed over the

GOES infrared (IR) image for the region containing tropical storm Emily valid at 0001 UTC 22 September 1987. This simulation uses an adiabatic initialization with 4 vertical modes. Note in Figs 2 and 3 that the height and divergence fields show no development whatsoever in the immediate vicinity of Emily. No precipitation is associated with this flow. However, some precipitation does occur over elevated topographical features in association with changes in the diurnal cycle.

Retrieved heating rates for Emily, based on the physical retrieval and regression procedures described in section 2, provides a knowledge of both the horizontal and vertical distribution of the diabatic heating. This information is then used directly in the CIMSS model diabatic initialization and diabatic forcing procedures, as described in section 3. Diabatic forcing, beginning at time step 120, i.e., at 1000 UTC 21 September 1987, and ending at time step 165, is applied during a forecast according to (2) through (7). The introduction contains a one and one-half hour ramp-up, with one and one-quarter hours of constant forcing, and a one hour ramp-down procedure. Thus, the diabatic forcing begins slowly ten hours into the forecast and shuts down 3.75 hours later. The length of the ramps can be adjusted based on model response. A tapered introduction and exit is necessary to keep gravity and inertia wave noise to a minimum.

At the end of the twenty-four hour forecast, or fourteen hours after the start of the forcing, the 700 mb geopotential heights contain several closed contour centers, as seen in Fig 4. Some indication of the development of a warm core is provided by the center containing the 3200 m contours. The convergence (negative divergence) at 700 mb (Fig 5) has a maximum of approximately -8×10^{-5} s^{-1} directly over the location of Emily. Also, the positive vorticity reaches a magnitude of 24×10^{-5} s^{-1} at 700 mb, as illustrated in Fig 6. The integrated precipitating liquid water, fourteen hours after the start of the diabatic forcing, has a maximum of 4.0 kgm^{-2} (Fig 7). However, smaller magnitudes are found in the SSM/I physical retrieval, shown in Fig 8, which contains a maximum near 2.5 kgm^{-2} of precipitating liquid and ice. Also, the spatial distribution for the retrieved precipitating field shows a comma shape. The lack of spatial structure in the forecasted quantity is though to be linked to a common feature among models, namely, a tendency to over-

develop precipitation situations. Too much condensation occurs in grid scale explicit cloud calculations because moist and dry downdrafts, which help to restrict the total condensation, are not correctly parameterized. Inadequacies in the vertical and horizontal mixing or turbulence parameterization, too coarse of a grid resolution, and other deficiencies in the cloud and rain water parameterizations may also be contributing factors. To help keep the storm from over developing or developing too rapidly, in our calculations the maximum amount condensed at any one time step at any grid location is restricted by requiring that $0 < |Q/fq| < 0.5$, where f is the Coriolis parameter and q the mixing ratio. Conservation of moisture is retained since the excess is carried in the slightly super saturated mixing ratio. This is thought to be a better alternative than using artificial diffusion, which is non-conservative, in our 40 km resolution simulations.

The remotely retrieved heating rate information described in section 2 is used in a fourteen hour forecast containing a diabatic initialization followed by two hours (24 time steps) of diabatic forcing. Four vertical modes are used in this simulation since, as described in our earlier work, the combined diabatic initialization and diabatic forcing is not sensitive to the choice of the vertical wave number in the vertical mode initialization (Bourke and McGregor 1983).

Results from the fourteen hour forecast are shown in Figs 9 through 12. The forecasted 700 mb height field contains two centers with closed contours (Fig 9). For the same time period, convergence (-1.2×10^{-5} s^{-1}) is found over this region (Fig 10) associated with a positive vorticity that has a maximum value of 16×10^{-5} s^{-1} (Fig 11). This development, that coincides with Emily, is somewhat less than that shown in Figs 4 through 8 primarily because the length of the forcing is less. This weaker signal is also evident in the integrated rain water shown in Fig 12, when compared with the values shown in Fig 7. Dispite having less integrated rain water, the weaker system has more rainfall at the surface during the first few hours of its existence, presumely because the clouds are closer to the surface and because the weaker vertical motions do not greatly impede the precipitating liquid.

5. Summary

Vertical heating profiles (1000 UTC 21 September 1987) are constructed using the vertical layer-mean latent heating rates from a cloud ensemble model and the slant path-integrated liquid and ice precipitating water contents retrieved from the SSM/I. This information is then used in a diabatic initialization and/or diabatic forcing procedure to help encourage the spin-up the precipitation and the development of tropical storm Emily. The robust nature of the diabatic forcing procedure, as described and tested in chapter 1 of this final report, is evident by the successful generation of a disturbance in both the twenty four and fourteen hour forecasts. One additional case study should be done to complete our investigation, after which the diabatic forcing procedure should be tested in an operational setting where many different meteorological situations can occur. The physical retrieval technique for estimating the vertical structure of the latent heating looks extremely promising.

Acknowledgments. This work was supported by NASA Grant NAGW-1855. One author (WHR) was supported in part by National Science Foundation Grant ATM-8920508.

References

Bourke, W. and J. L. McGregor, 1983: A nonlinear vertical mode initialization scheme for a limited area prediction model. *Mon. Wea. Rev.*, **111**, 2285-2297.

Donner, L. J., 1988: An initialization for cumulus convection in numerical weather prediction models. *Mon. Wea. Rev.*, **116**, 377-385.

Errico, R. and P. J. Rasch, 1988: A comparison of various normal-mode initialization schemes and the inclusion of diabatic processes. *Tellus*, **40A**, 1-25.

Fiorino, M and T.T. Warner, 1981: Incorporating surface winds and rainfall rates into the initialization of a mesoscale hurricane model. *Mon. Wea. Rev.*, **109**, 1914-1929.

Hoke, J. E. R. A. Anthes, 1976: The initialization of numerical models by a dynamical initialization technique. *Mon. Wea. Rev.*, **104**, 1551-1556.

Leslie, L. M., G. A. Mills, L. W. Logan, D. J. Gauntlett, G. A. Kelly, J. L. McGregor and M. J. Manton, 1985: A high resolution primitive equation NWP model for operations and research. *Aust. Meteor. Mag.*, **33**, 11-35.

McGregor, J. L., L. M. Leslie and D. J. Gauntlett, 1978: The ANMRC limited-area model: consolidated formulation and operational results. *Mon. Wea. Rev.*, **106**, 427-438.

Salmon, E. M., and T. T. Warner, 1986: Short-term numerical precipitation forecasts initialized using a diagnosed divergent-wind component. *Mon. Wea. Rev.*, **114**, 2122-2132.

Tao, W-K., J. Simpson, S. Lang, M. McCumber, R Adler and R. Penc, 1990: An algorithm to estimate the heating budget from vertical hydrometer profiles. *J. Appl. Meteor.*, **29**, 1232-1244.

Tarbell, T. C., T. T. Warner and R. A. Anthes, 1981: An example of the initialization of the divergent wind component in a mesoscale numerical weather prediction model. *Mon. Wea. Rev.*, **109**, 77-95.

Turpeinen, O. M., L. Garand, R. Benoit and M. Roch, 1990: Diabatic initialization of the Canadian regional finite-element (RFE) model using satellite data. Part I: Methodology and application to a winter storm. *Mon. Wea. Rev.*, **118**, 1381-1395.

Table 1. Latent heating rate regression formulae coefficients and statistics. Note that there are insufficient data to perform a regression at the two highest levels. Units of altitude are kilometers, and bias and σ_{err} are in joules/m^3-s.

altitude	a_1	a_2	bias	σ_{err}	r
0.56	0.370	-0.251	-0.073	0.430	0.617
1.69	0.909	-0.355	-0.087	0.942	0.528
2.82	0.108	-0.122	0.066	0.478	0.229
3.94	0.227	-0.119	0.018	0.532	0.305
5.07	0.344	0.044	0.007	0.289	0.607
6.19	0.166	0.168	0.008	0.185	0.786
7.32	0.045	0.181	0.007	0.139	0.841
8.45	0.059	0.123	0.007	0.112	0.809
9.57	0.044	0.072	0.009	0.062	0.853
10.70	0.038	0.025	0.006	0.054	0.650
11.82	0.045	-0.003	0.006	0.065	0.436
12.95	0.170	-0.022	0.022	0.162	0.576
14.08	0.041	-0.007	0.002	0.049	0.461
15.20	-0.002	0.000	-0.000	0.002	0.545
16.33	-0.000	0.000	0.000	0.000	0.443
17.45	----	----	----	----	----
18.58	----	----	----	----	----

List of Figures

Fig. 10. Same as Fig 9 but showing the divergence. Contour interval is 1×10^{-5} s^{-1}.

Fig. 11. Same as Fig 9 but showing the vorticity. Contour interval is 4×10^{-5} s^{-1}.

Fig. 12. The vertically integrated rain water x 10 associated with the fields shown in Fig 9, 10 and 11. Contour interval is 0.5 kgm^{-1}.


700 MB DIABATIC TEMPERATURE EQUIVALENT X 100
0003 GOES-7 IR 08 21 SEP 87264 100100 04057 08121 04.00

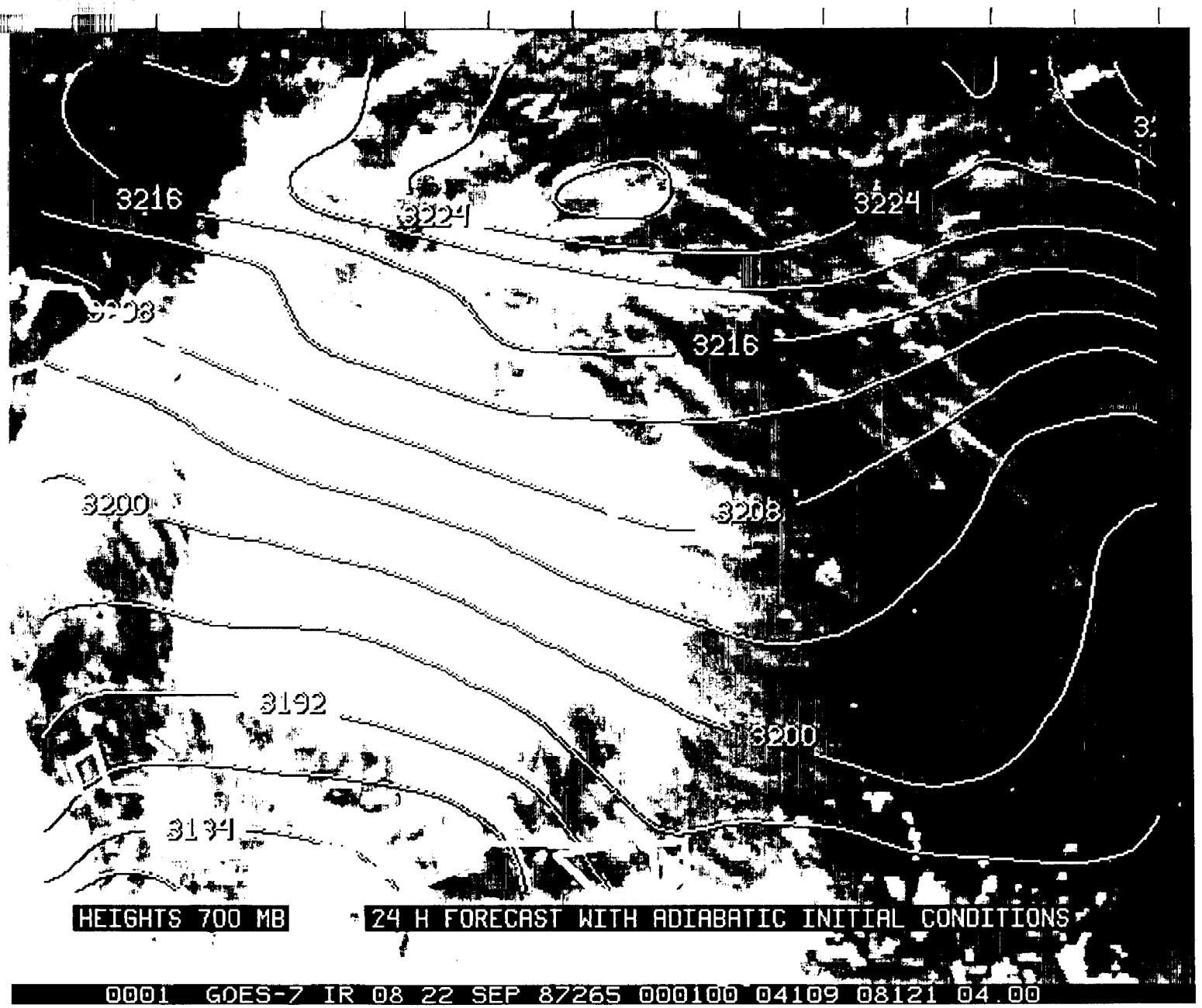
3216
3224
3224
3216
3200
3208
3192
3200
3184
HEIGHTS 700 MB
24 H FORECAST WITH ADIABATIC INITIAL CONDITIONS
0001 GOES-7 IR 08 22 SEP 87265 000100 04109 08121 04.00

Fig 2

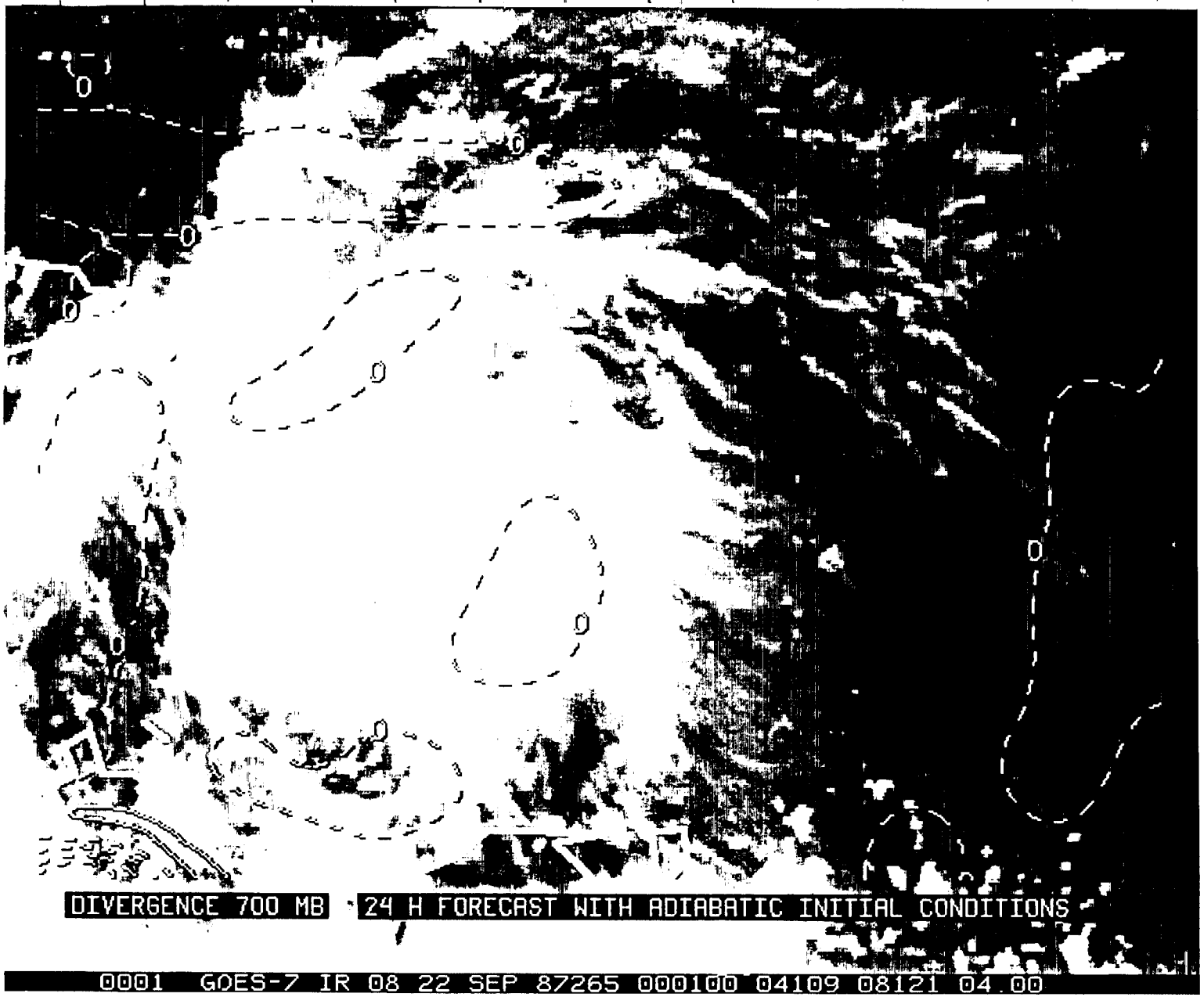
0
0
0
0
0
0
0
0
0
DIVERGENCE 700 MB
24 H FORECAST WITH ADIABATIC INITIAL CONDITIONS
0001 GOES-7 IR 08 22 SEP 87265 000100 04109 08121 04.00

Fig 3

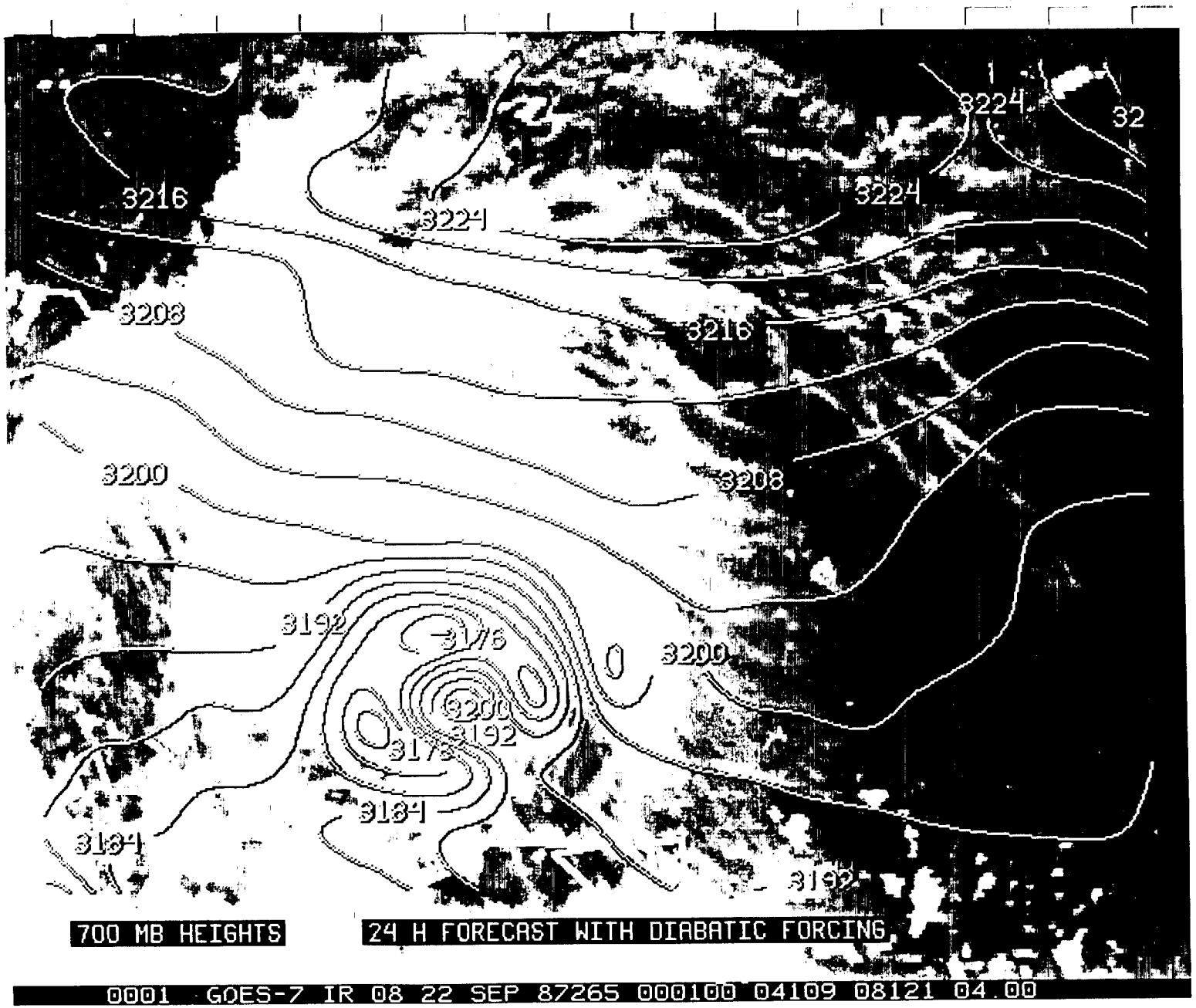
3224
32
3216
3224
3224
3208
3216
3200
3208
3192
3176
3200
3200
3192
3176
3184
3184
3192
700 MB HEIGHTS
24 H FORECAST WITH DIABATIC FORCING
0001 GOES-7 IR 08 22 SEP 87265 000100 04109 08121 04.00

Fig 4

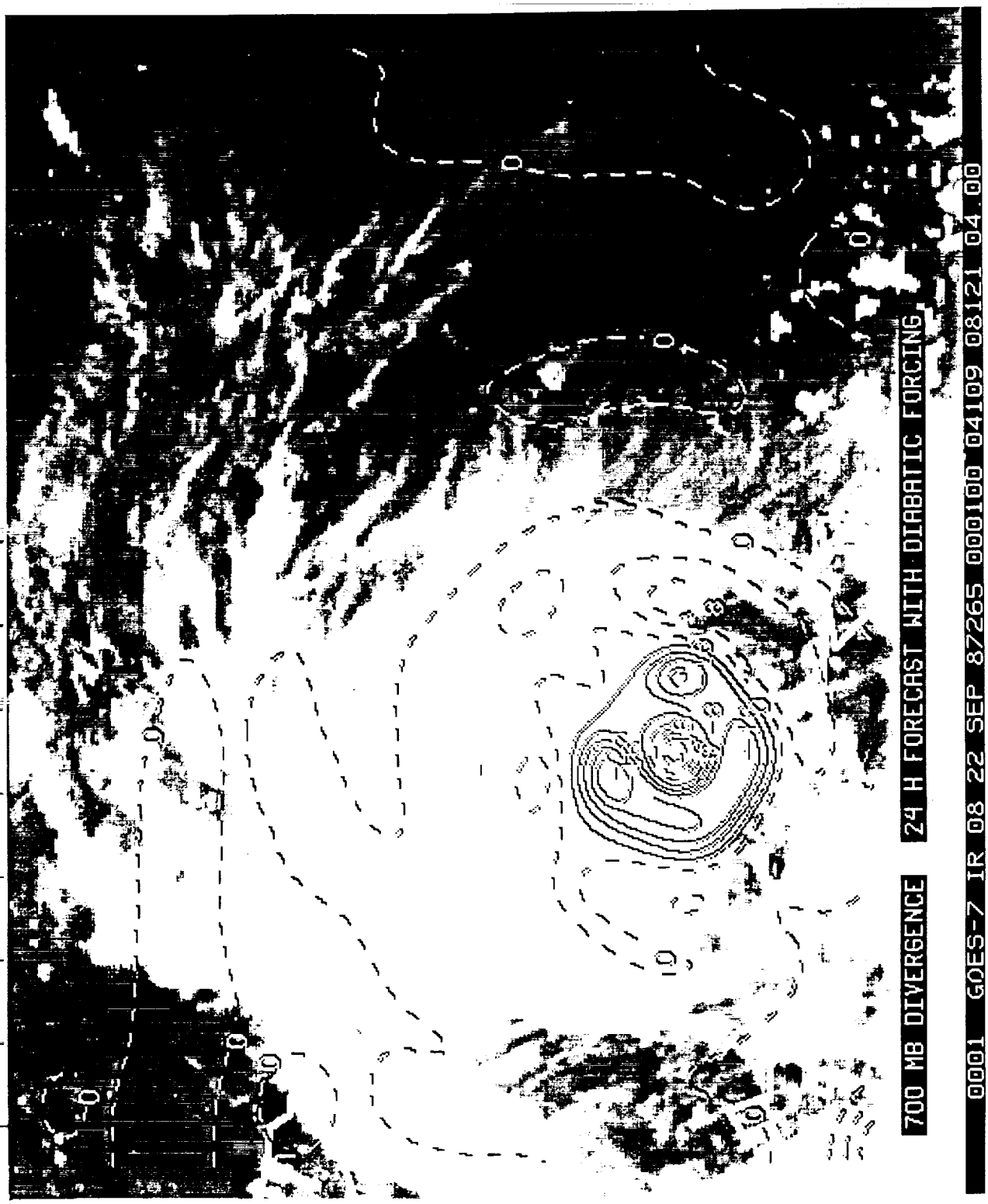
0001 GOES-7 IR 08 22 SEP 87265 000100 04109 08121 04 00
700 MB DIVERGENCE
24 H FORECAST WITH DIABATIC FORCING

Fig 5

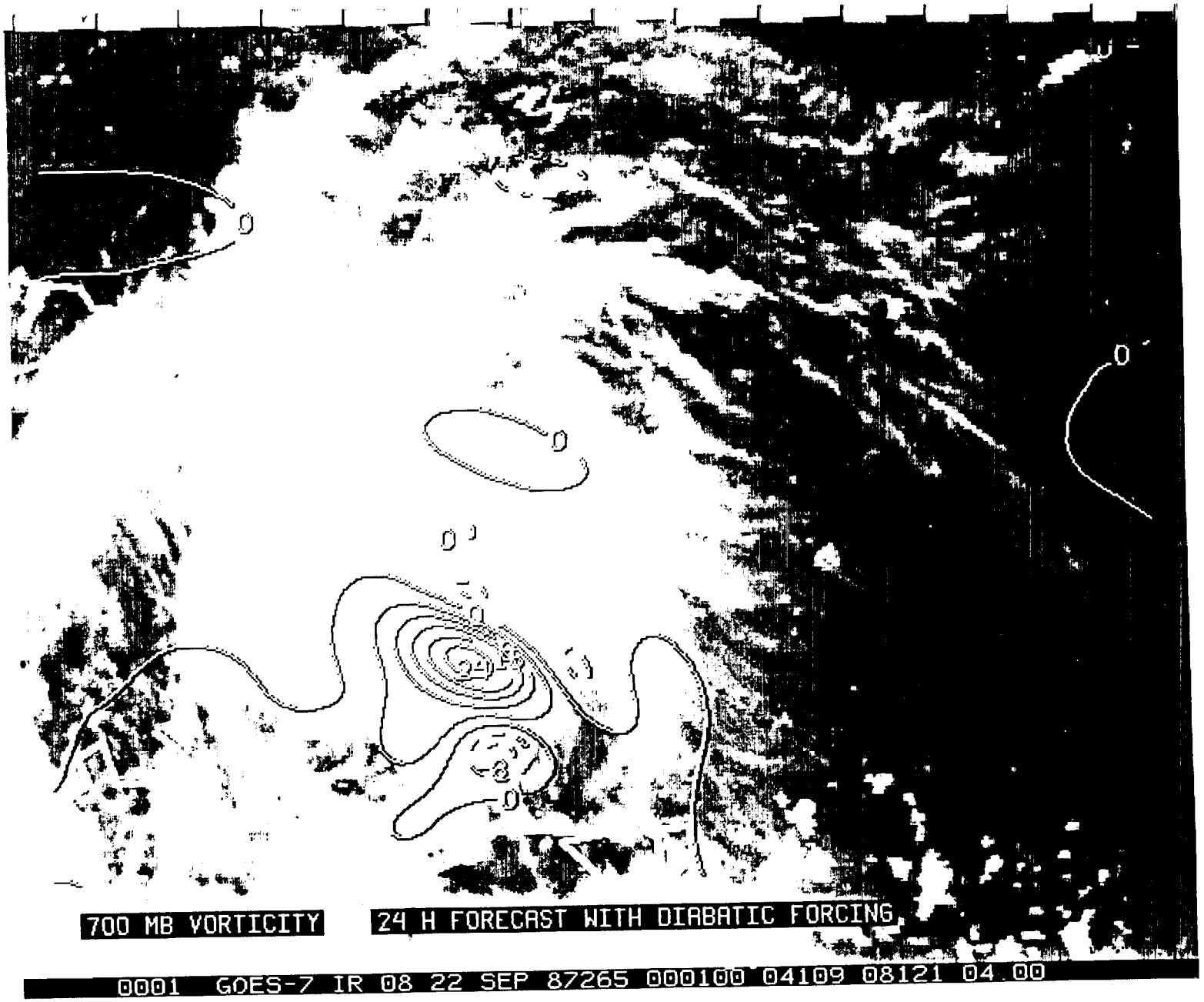
700 MB VORTICITY
24 H FORECAST WITH DIABATIC FORCING
0001 GOES-7 IR 08 22 SEP 87265 000100 04109 08121 04 00

Fig 1

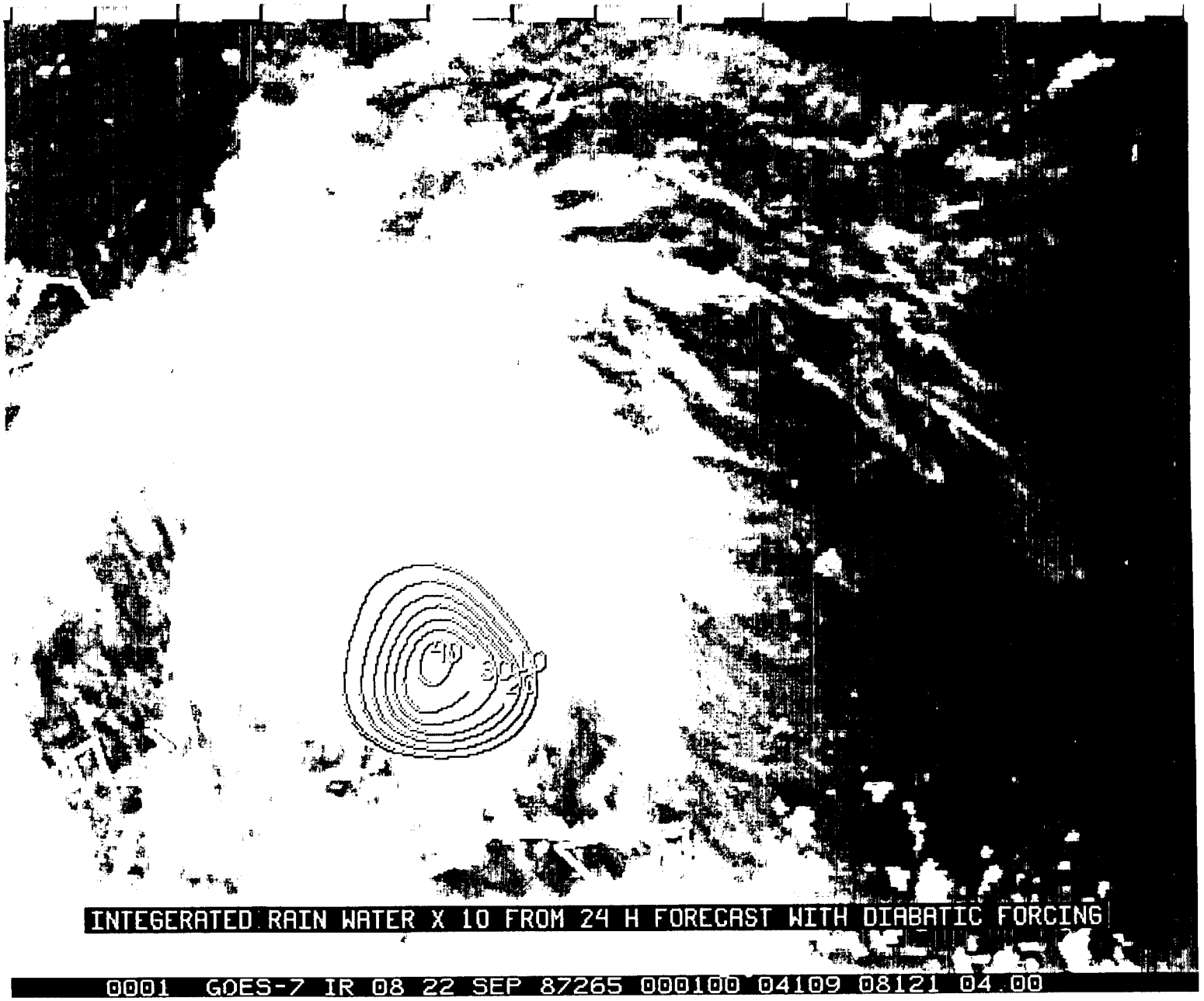
INTEGERATED RAIN WATER X 10 FROM 24 H FORECAST WITH DIABATIC FORCING
0001 GOES-7 IR 08 22 SEP 87265 000100 04109 08121 04 00

Fig 7

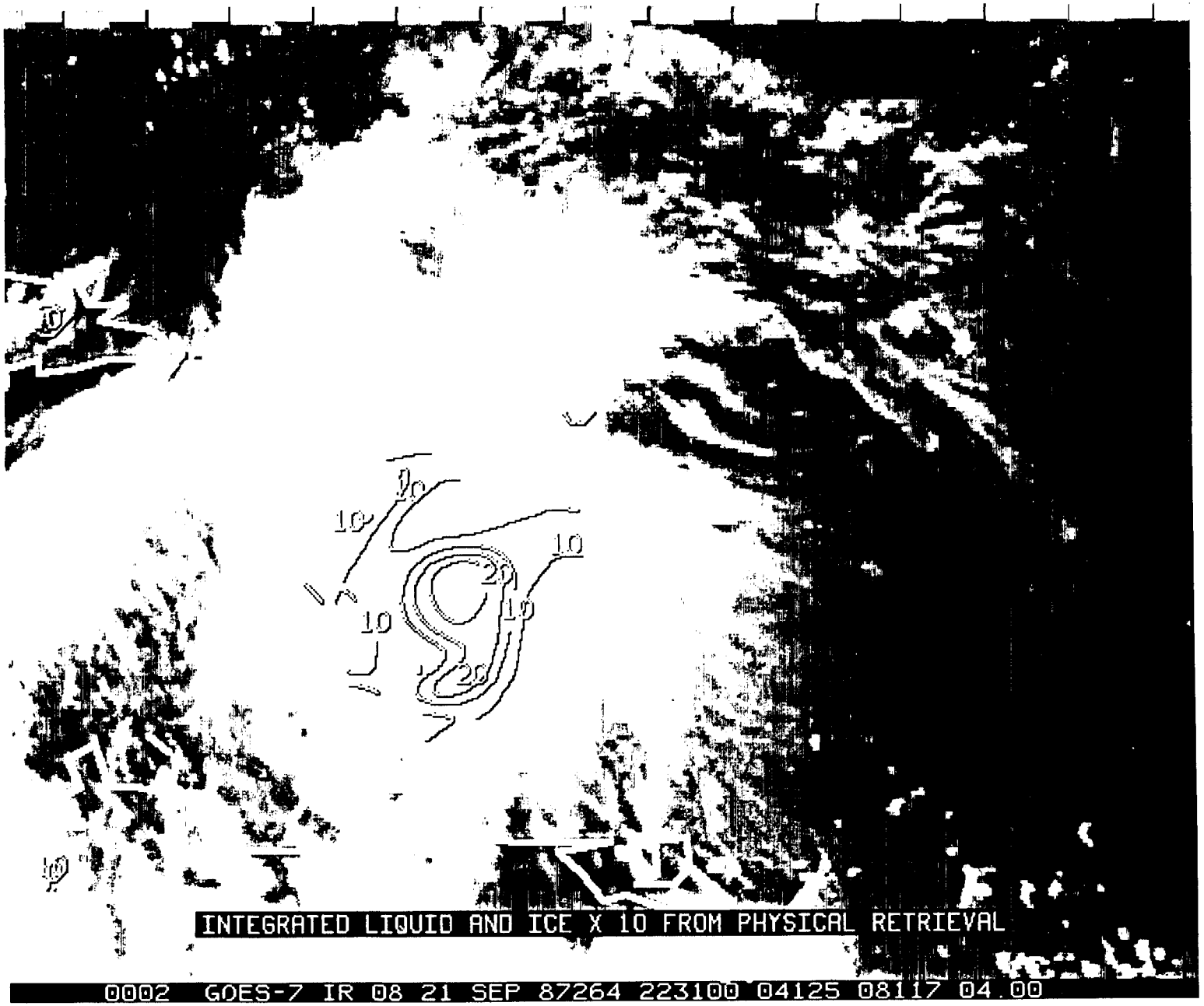
10
10
10
10
20
10
20
10
INTEGRATED LIQUID AND ICE X 10 FROM PHYSICAL RETRIEVAL
0002 GOES-7 IR 08 21 SEP 87264 223100 04125 08117 04.00

Fig 2

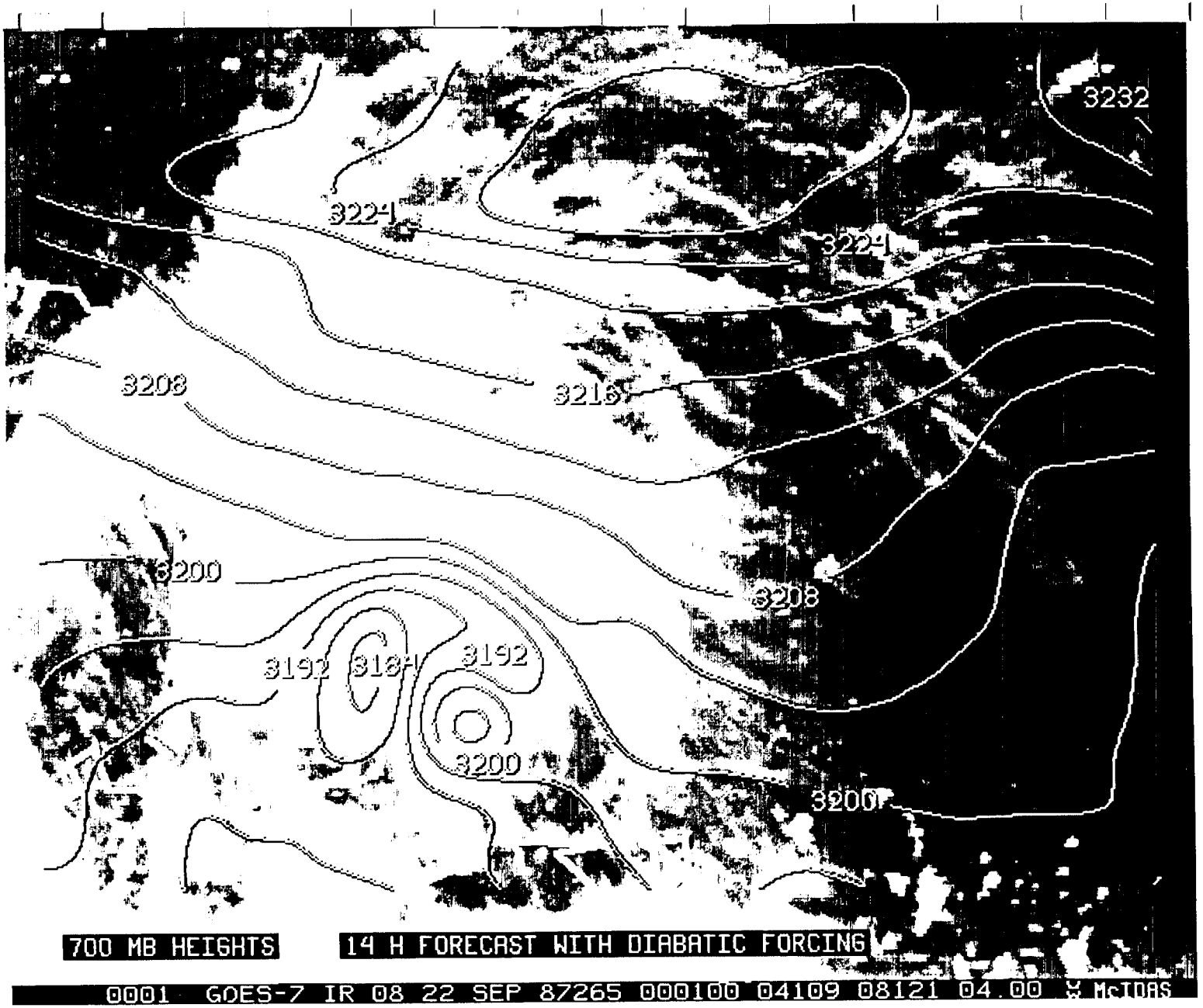
3232
3224
3224
3208
3216
3200
3208
3192
3184
3192
3200
3200
700 MB HEIGHTS
14 H FORECAST WITH DIABATIC FORCING
0001 GOES-7 IR 08 22 SEP 87265 000100 04109 08121 04.00 McIDAS

Fig 9

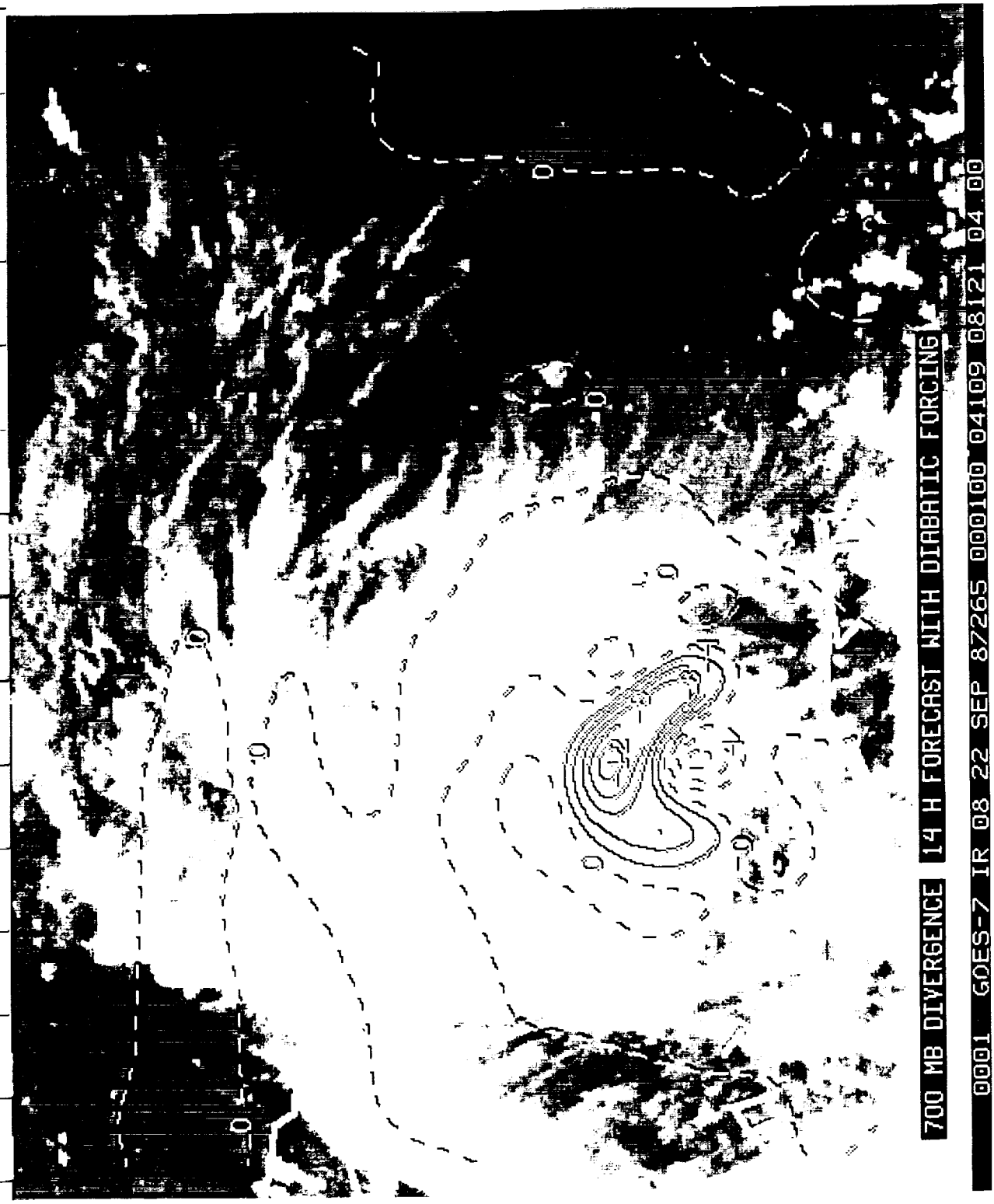
700 MB DIVERGENCE
14 H FORECAST WITH DIABATIC FORCING
0001 GOES-7 IR 08 22 SEP 87265 000100 04109 08121 04 00

Fig 10

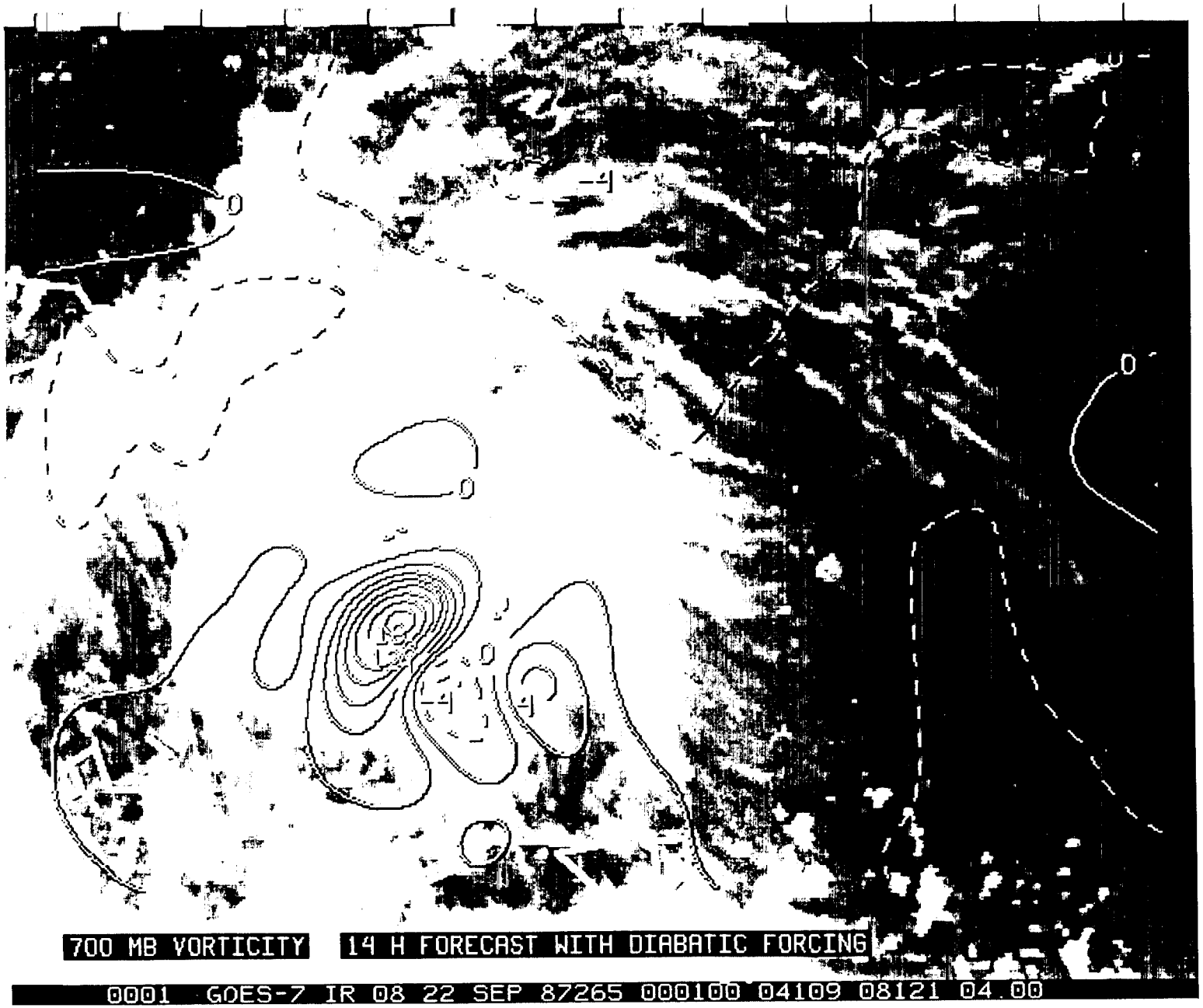
700 MB VORTICITY
14 H FORECAST WITH DIABATIC FORCING
0001 GOES-7 IR 08 22 SEP 87265 000100 04109 08121 04 00

Fig 11

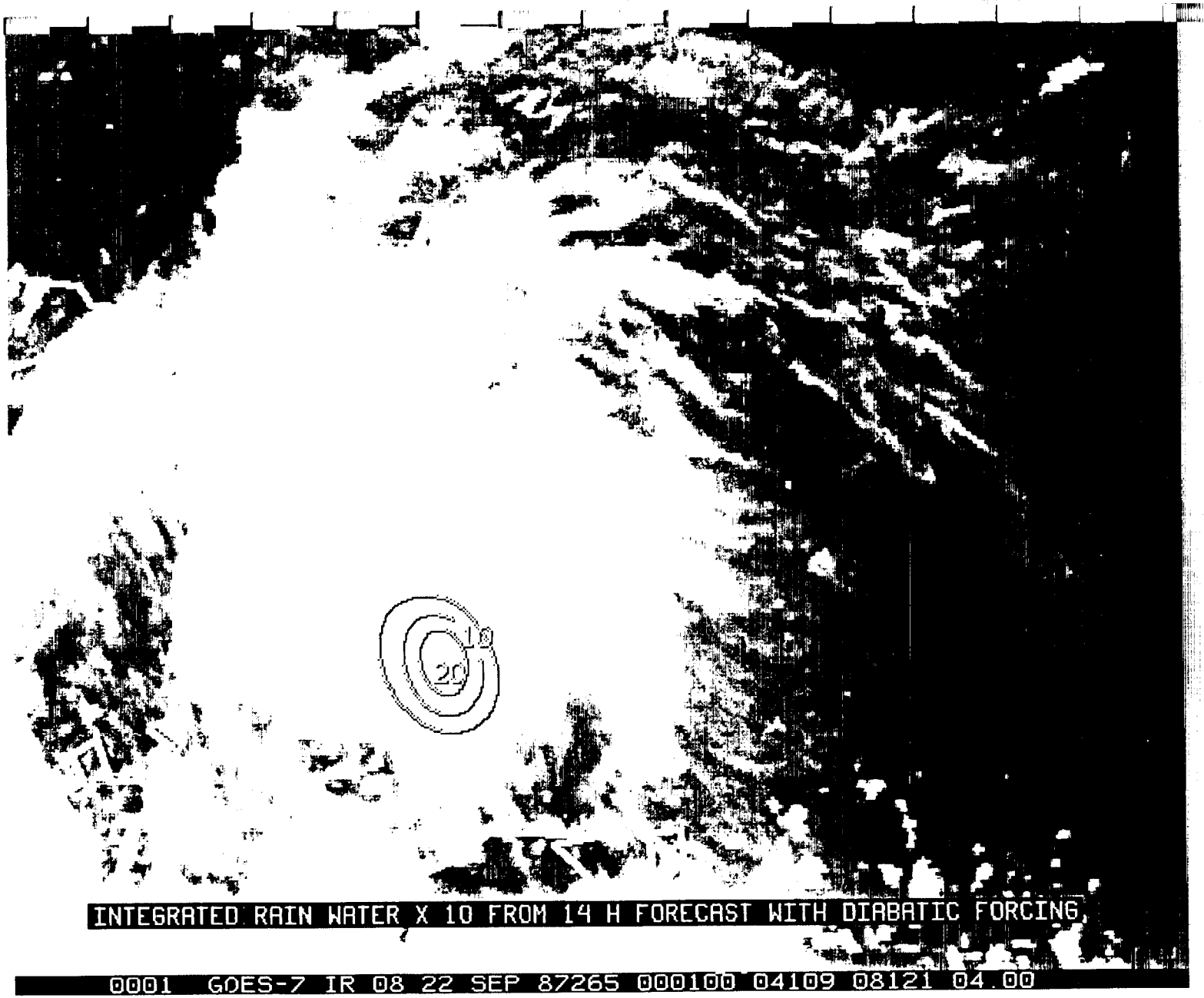
10
20
INTEGRATED RAIN WATER X 10 FROM 14 H FORECAST WITH DIABATIC FORCING
0001 GOES-7 IR 08 22 SEP 87265 000100 04109 08121 04.00

Fig 12